Iraqi Journal of Physics, 2026 *Vol. 24, No.1, PP.121-131*
https://doi.org/10.30723/ijp.v23i2.1346 *P-ISSN: 2070-4003*
E-ISSN: 2664-5548

Effect of Concentration on the Structural and Optical Properties of ZnS Thin Films Deposited by the Spray Pyrolysis Technique

Hiba K. Abood[1*] and Nathera A. Ali[1]
[1]*Department of Physics, College of Science, University of Baghdad, Baghdad, Iraq*
[*]Corresponding author: Nathera.Ali@sc.uobaghdad.edu.iq

Abstract
Zinc sulfide (ZnS) thin films were deposited on glass substrates using the spray pyrolysis technique (SPD) with different precursor concentrations (10^{-4} to 10^{-1}M). The structural, morphological, compositional, and optical properties were investigated using X-ray diffraction (XRD), atomic force microscopy (AFM), scanning electron microscopy (SEM), energy dispersive X-ray spectroscopy (EDX), Fourier transform infrared spectroscopy (FTIR), and UV-Vis spectroscopy. XRD results revealed a transformation from amorphous to crystalline cubic ZnS structure with increasing precursor concentration. FESEM and AFM analyses showed that higher concentrations produced smoother surfaces with smaller particle sizes. EDX confirmed improved stoichiometry at higher concentrations. The optical band gap decreased from 4.16 to 3.21 eV as concentration increased, indicating improved crystallinity. The results demonstrate the precursor concentration significantly influences the structural and optical properties of ZnS thin films.

Article Info.

Keywords:
ZnS Thin Films, Different Concentration, Spray Pyrolysis, Structural Properties, Optical Properties.

Article history:
Received: Jul. 11, 2024
Revised: Jan. 30, 2025
Accepted: Feb.14, 2025
Published:Mar.01,2026

1. Introduction
Zinc sulfide (ZnS) is a an important II-VI semiconductor material that has attracted considerable attention due to its unique physical and optical properties. These include a wide direct band gap (~ 3.5 eV), low toxicity, high optical transparency in the visible region, and good chemical stability [1-2]. ZnS thin films can be prepared using several deposition techniques, including pulsed laser deposition [3], chemical bath deposition [4, 5], chemical vapor deposition [6], electrodeposition [7], and spray pyrolysis [8, 9]. Among these techniques, spry pyrolysis has gained significant interest due to its simplicity, low cost, stability, and suitability for large area deposition [10,11]. Moreover, this method has been successfully applied to various semiconductor materials such as SnO_2 [12], ZnO [13], $CuInS_2$ [14], and $MnIn_xS_4$ [15] Owing to these properties, ZnS has been widely employed in various optoelectronic applications such as solar cells, photodetectors, light-emitted diodes (LEDs), laser diodes, and flat-panel displays [16-18].

ZnS exists in two primary crystalline phases: cubic zinc blend and hexagonal wurtzite structure [19, 20]. The cubic phase is thermodynamically stable under normal conditions, whereas the hexagonal phase is typically formed at higher temperatures. The structural phase strongly influences the optical and electronic properties of the materials. In general, the optical properties of ZnS thin films are influenced by several factors, including precursor concentration, deposition parameters, crystallinity, and film thickness. ZnS thin films are highly transparent in the visible region and exhibit strong photoluminescence emission, making them promising materials for optoelectronic and photovoltaic applications [21-23].

2. Methodology
Zinc acetate was used as the zinc precursor and thiourea (NH_2CSNH_2) was used

as the sulfur source to prepare ZnS thin films. Appropriate amounts of zinc acetate and thiourea were dissolved separately in 200 mL distilled water under continuous magnetic stirring for 15 minutes to prepare aqueous precursor solutions. For every precursor solution, four different molar concentrations (10^{-4}, 10^{-3}, 10^{-2}, and 10^{-1} M) were prepared. The solutions were sprayed on clean glass substrates using a spray pyrolysis system. The temperature of the substrate was held at 400 °C while during deposition, a fixed distance of 26 cm from nozzle to substrate surface was kept.

The structural, morphological, compositional, and optical characteristics of the ZnS thin films were assessed after the deposition using X-ray diffraction (XRD), scanning electron microscopy (SEM), atomic force microscopy (AFM), Fourier transform infrared spectroscopy (FTIR), and UV–Visible spectrophotometry techniques.

3. Results and Discussion

3.1. XRD Analysis

The X-ray diffraction (XRD) patterns of ZnS thin films deposited at various precursor concentrations by the spray pyrolysis technique are shown in Fig. 1. The comparison clearly shows the effect of precursor concentration on the film's structural evolution. Both films made at 1×10^{-4} and 1×10^{-3} M (Fig. 1a and b) have broad diffraction patterns without clear peaks, The lack of discernible sharp diffraction peaks indicates the absence of long-range crystalline order in the films. Such behavior is attributed to low precursor concentration, resulting in limited nucleation density and crystal growth during deposition. Moreover, the deposition rate at these concentrations was relatively low, which may have contributed to an even thinner film, further inhibiting crystallization. Meanwhile, the film deposited at 1×10^{-2} M (Fig. 1c) exhibits a diffraction peak on the (111) plane, which indicates crystallization begins. Increasing the concentration to 1×10^{-1} M (Fig. 1d) causes four clear diffraction peaks at 2θ of 28.84°, 34.45°, 48.13°, and 56.90° corresponding to (111), (200), (220), and (311) crystallographic planes, respectively. The intensity of these peaks is in accord with the standard JCPDS Card No. 05-0566, indicating that cubic ZnS phase (Space Group $P4_3m$) was obtained [24-27]. As precursor concentration increases, the large number and high intensity of diffraction peaks imply an increase in crystallinity and structural refinement. This improvement is attributed to a higher availability of reactant species, which facilitates nucleation and grain growth. In addition, increased precursor concentration probably leads to higher film thickness and deposition rate.

When attempting to determine the size of the crystallites based on the XRD data, the Debye-Scherrer formula is usually utilized is given in Eq. (1) [25]:

$$D = \frac{k\lambda}{\beta \cos\theta} \qquad (\mathbf{1})$$

where D represents the size of the crystallite, k represents the form factor, λ represents the wavelength of the X-ray, β represents the half maximum intensity in radians, and θ represents the Bragg angle. When calculating the form factor, k, the shape of the crystallites is considered, and the value of this factor is determined by the crystal structure. Table 1 contains a comprehensive listing of the X-ray diffraction parameters of ZnS thin films.

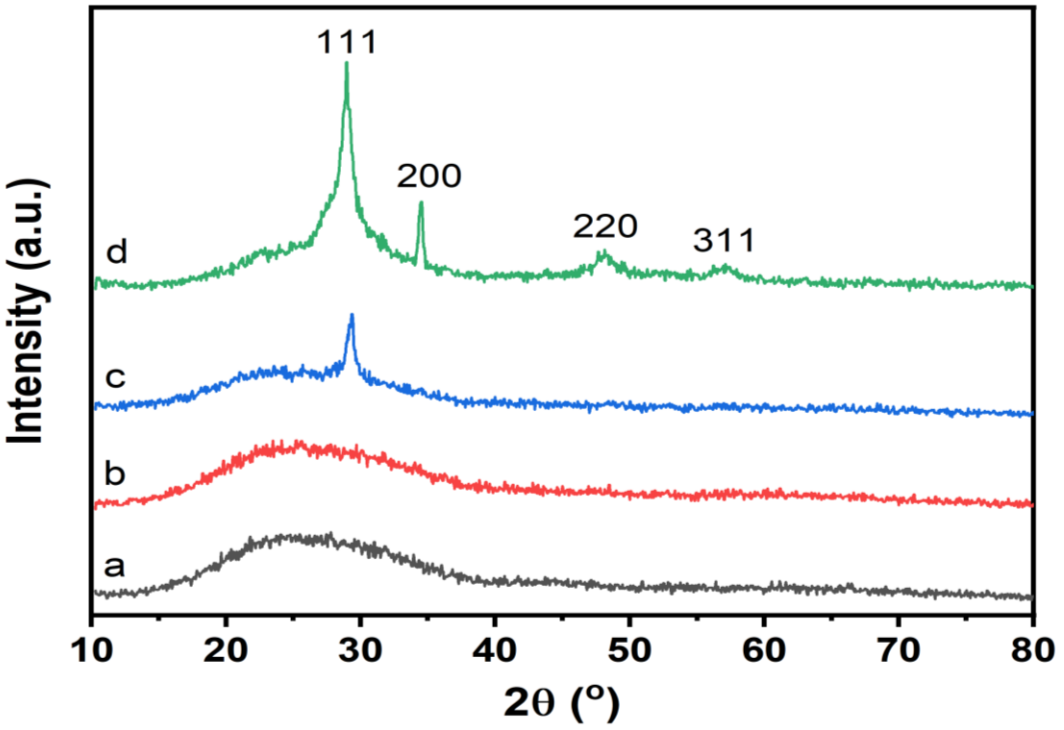

Figure 1: XRD of ZnS thin films at a) 1×10^{-4} mol and b) 1×10^{-3} c) 1×10^{-2} and d) 1×10^{-1} mol of zinc chloride and thiourea.

Table 1. XRD parameters of ZnS thin films

hkl	2θ (°)	β (°)	d-spacing (Å)	D (nm)	
1×10^{-2}	111	29.12	0.62	3.05373	13.8
1×10^{-1}	111	28.84	0.83	3.09335	10.3

3.2. Field Emission Scanning Electron Microscope (FESEM)

Fig. 2 SEM micrographs of ZnS thin films deposited at various precursor concentrations. At the lowest concentration (1×10^{-4} M), the surface of the film seems non-homogeneous and rather rough, with ill-defined features, revealing only a limited nucleation process followed by an incomplete formation of the film. This morphology indicates limited precursor availability, leading to lower deposition rate and grain growth inhibition. At 1×10^{-3} M concentration, the surface was relatively denser and began to form domains of granular structures. This transition indicates the commencement of nucleation and early-stage crystallite formation, because an increased precursor concentration will yield a larger pool of reactive species to drive crystalline growth. At 1×10^{-2} M, a uniform and denser surface was identified with defined grain distribution showing better film coverage and an overall crystallinity improvement. Compared with the control and lower concentrations, higher concentration (1×10^{-1} M) showed a clear increase in grain sizes, microstructure exhibiting even larger grains with sharper edges which indicated an increase in crystallite growth and improved structural ordering.

The SEM observations support that increasing precursor concentration favors nucleation and growth of grains resulting in more compact films with enhanced uniformity and pronounced crystalline features. This morphological transformation correlates well with the XRD data confirming the conversion of amorphous to crystalline ZnS with increasing precursor concentration.

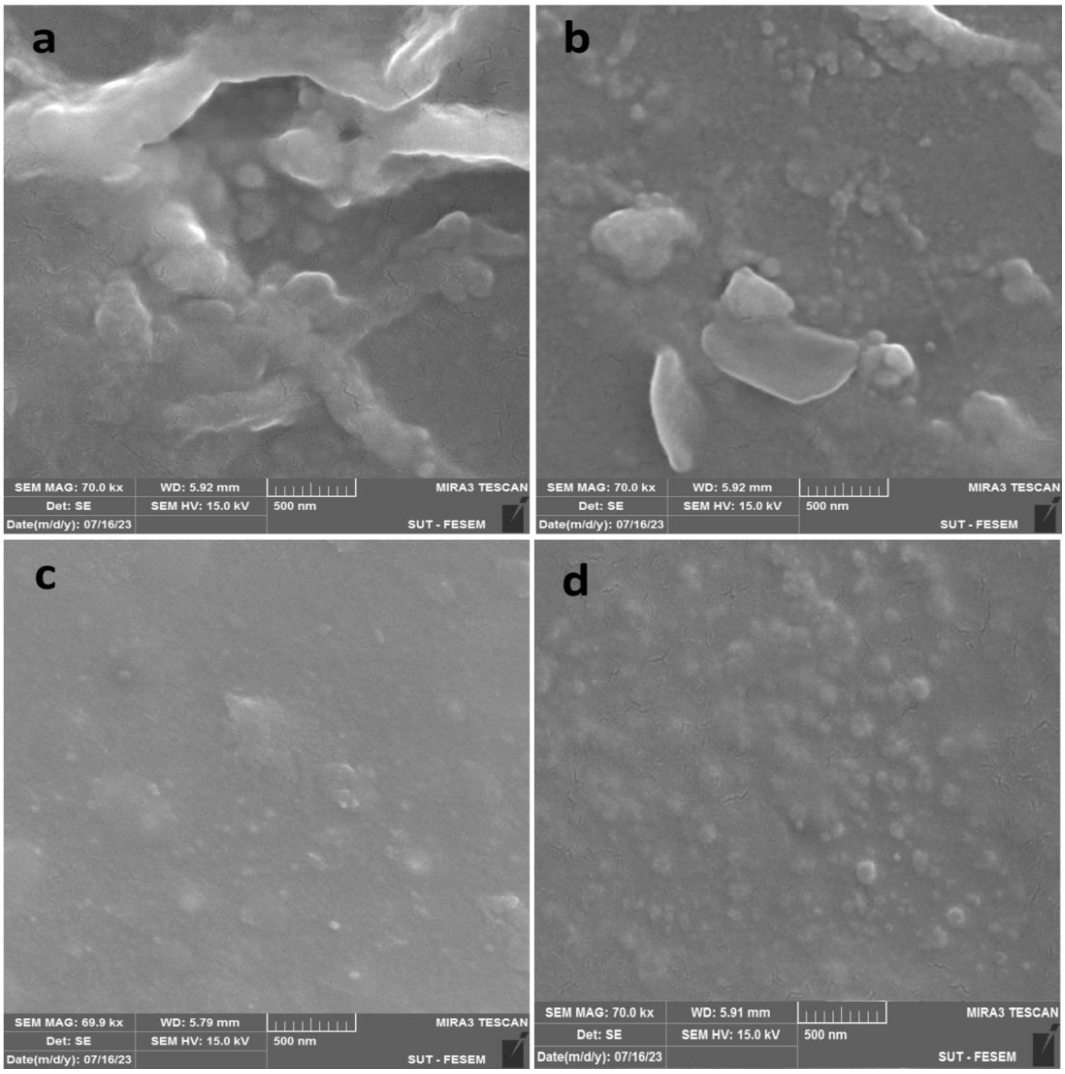

Figure 2: The FESEM of ZnS thin films at precursors concentration of (a) 1×10^{-4}, (b) 1×10^{-3}, (c) 1×10^{-2} and (d) 1×10^{-1} mol of zinc chloride and thiourea.

Table 2 shows the elemental composition of ZnS thin films, which were analyzed using energy-dispersive X-ray spectroscopy (EDX) as illustrated in Fig. 3. The presence of Zn, S and O all appear in the spectra for each sample. The film prepared with the lowest precursor concentration (1×10^{-4} M) showed a high oxygen content and very low sulfur concentration, suggesting that only partial formation of ZnS had occurred, possibly followed by oxidation of the film surface owing to inadequate precursor availability. When the precursor concentration increased to 1×10^{-3} M, the oxygen content decreased further and the Zn and S contents were higher than before, indicating better formation of ZnS phase. The oxygen content was greatly reduced at a rise to 1×10^{-2} and 1×10^{-1} M, with a significant increase in the atomic percentages of zinc (Zn) and sulfur (S). At the highest concentration (1×10^{-1} M), sulfur was at 24.87 wt. % and zinc became the main element at 67.85 wt.%. The gradual decrease of

oxygen followed by the increase in the Zn and S concentrations demonstrates stronger bond formation between Zn–S and better film stoichiometry at a higher precursor concentration. This evolutionary composition also confirms the previous suggestions that growing at higher precursor concentrations may diminish oxygen incorporation, therefore leading to triggered formation process of well-formed and more perfect ZnS thin films which are corroborated by XRD and SEM results.

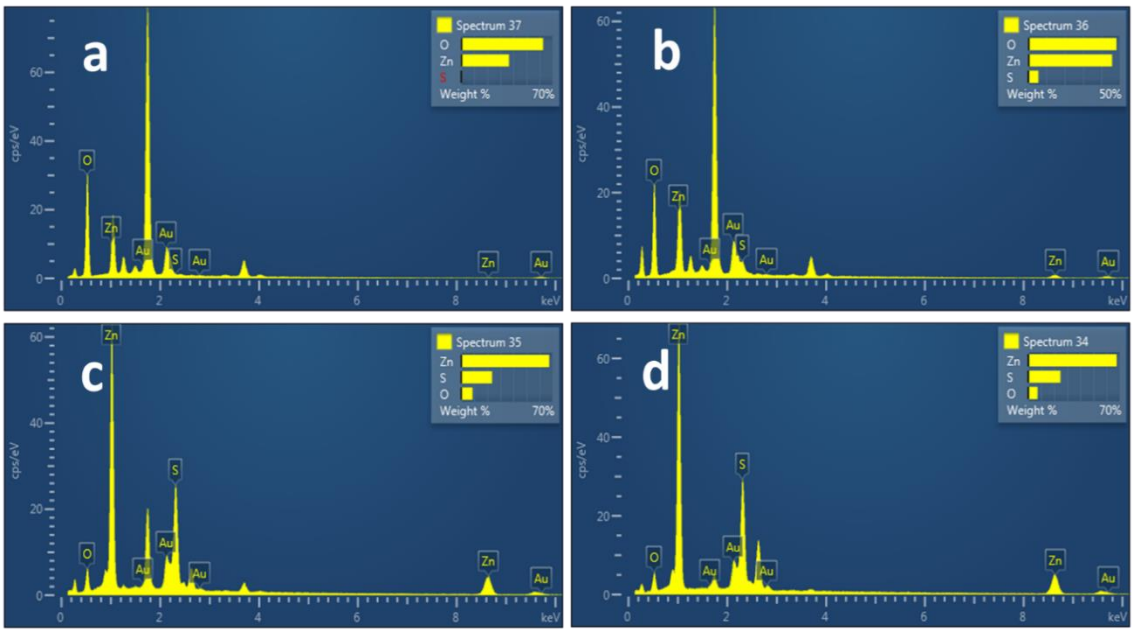

Figure 3. EDX of ZnS thin films at precursors concentrations: (a) 1×10^{-4}, (b) 1×10^{-3}, (c) 1×10^{-2} and (d) 1×10^{-1} mol of zinc chloride and thiourea.

Table 2: EDX results of ZnS thin films.

Element	Sample							
	1×10^{-4}		1×10^{-3}		1×10^{-2}		1×10^{-1}	
	W%	A%	W%	A%	W%	A%	W%	A%
O	62.83	87.22	48.35	77.44	8.74	23.56	7.28	20.06
S	0.42	0.29	5.69	4.55	23.75	31.93	24.87	34.19
Zn	36.75	12.48	45.96	18.01	67.50	44.51	67.85	45.75

3.3. Atomic Force Microscopy (AFM)

Surface morphology and roughness of ZnS thin films with different precursor amounts were studied using atomic force microscopy (AFM). The two-dimensional AFM images, three-dimensional AFM images and corresponding histograms of particle size distribution are presented in Fig. 4. Quantitative roughness parameters like arithmetic mean height (Sa), root mean square roughness (Sq), and maximum height (Sz) are listed in Table 3. Results show obvious correlative dependence of particle size and surface roughness on precursor concentration. In addition, as the concentration increased to 1×10^{-3} M, both average particle size (119.6 nm) and roughness parameters (Sq = 78.14 nm, Sa = 58.94 nm, Sz = 705.52 nm) showed a reduction indicating that film formed at lower mass fractions exhibit less surface uniformity compared with low mass fraction polymerization films.When the concentration was increased to 1×10^{-2} M, the size of the particles became significantly small i.e. 65.73 nm and roughness values also decreased (Sq = 24.13 nm, Sa = 19. At the highest concentration (1×10^{-1} M) of 14 h

with a smoothest surface and smallest particle size (39.03 nm), also showed Sq = 11.04 nm, and Sa = 7.96 nm. The less precursor, the more grains are formed which leads to a rougher surface. The improved crystal quality observed in the XRD data can be ascribed to these attributes: smaller particle size and more homogeneous surface at higher concentrations. In summary, precursor concentration is a significant factor in controlling the size of particles and surface morphology for ZnS thin films prepared by the spray pyrolysis method.

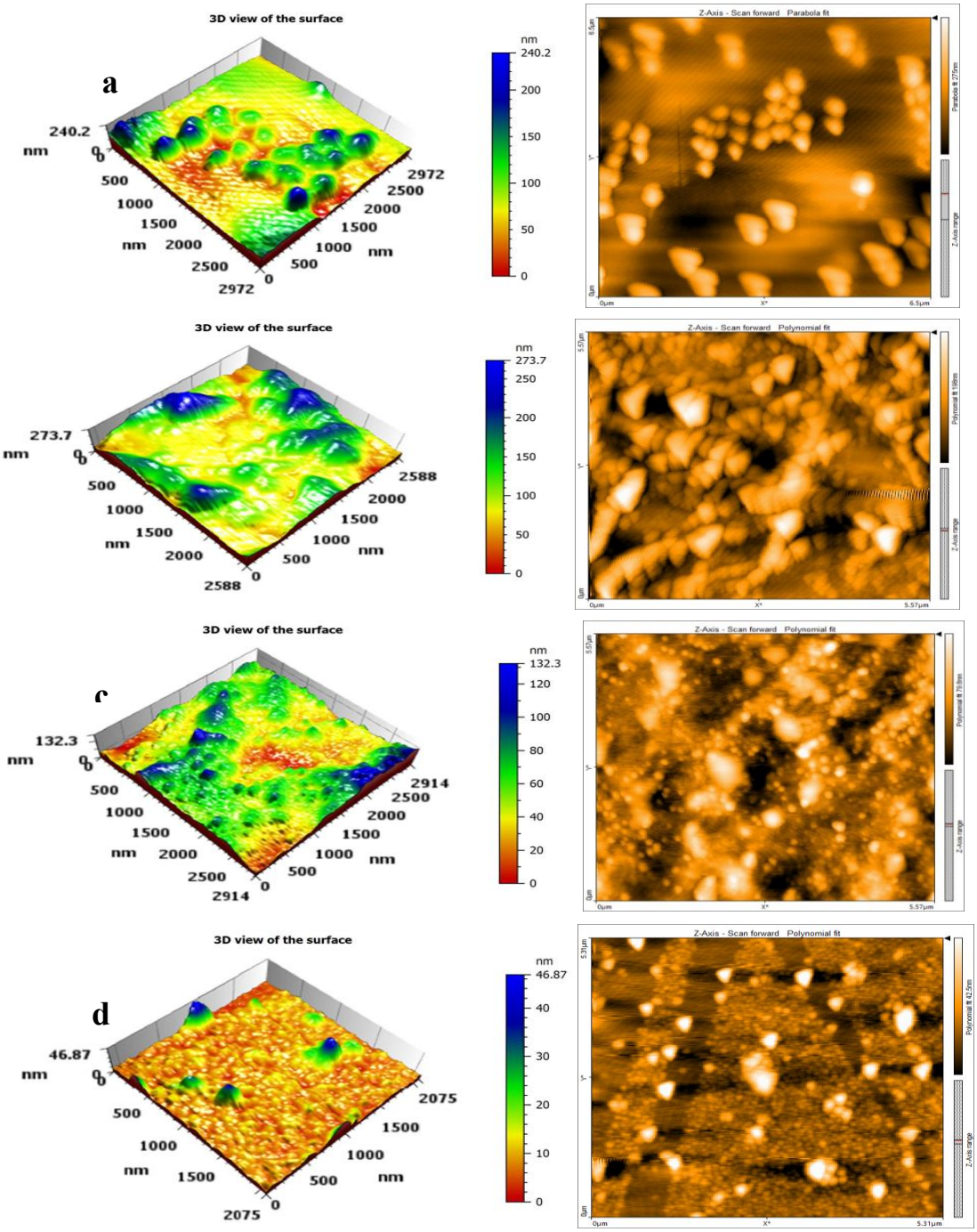

Figure 4: AFM and particle size distribution histogram of ZnS thin films at a) 1×10^{-4} mol and b) 1×10^{-3} c) 1×10^{-2} and d) 1×10^{-1} mol of zinc chloride and thiourea.

Table 3. AFM parameter of ZnS thin films

Sample	Particle analysis	Roughness analysis		
	Mean diameter (nm)	S_q (nm)	S_z (nm)	S_a (nm)
1×10^{-4}	187.2	76.12	584.3	58.21
1×10^{-3}	119.6	55.43	333.5	43.34
1×10^{-2}	65.73	24.13	162.1	19.39
1×10^{-1}	39.03	11.04	105.6	7.96

3.4. Optical Properties

Precursor concentrations from 1×10^{-4} to 1×10^{-1} M, with results demonstrating a gradual ramp in optical absorption as precursor concentration increases, as shown in Fig. 5. The film prepared at 1×10^{-4} M had the lowest absorbance, while higher concentrations showed a marked increase in absorbance, with the highest value attained at 1×10^{-1} M. Higher concentration increases the crystal quality resulting in thicker films, allowing the light to interact more with the films, leading to an increase in absorption. Since a higher concentration of precursors gives greater deposition rate and film density consequently more optical absorption occurs. Additionally, improved structural packing at higher concentration may facilitate electronic transitions near the band edge. The optical band gap (E_g) of the ZnS thin films was calculated with Tauc's relation for direct allowed transitions, Eq. (2) [28]:

$$(\alpha h\nu)^2 = A(h\nu - E_g) \quad \textbf{(2)}$$

where α is the absorption coefficient, hν is the photon energy, A is a constant and Eg represents optical band gap. We observe a clear decreasing trend in the band gap values calculated by UV-Vis spectroscopy with increasing precursor concentration as shown in Table 4 and illustrated in Fig. 6.

The film with the maximum band gap value, 4.16 eV, was observed for the deposited which had a molarity of 1×10^{-4} M. At 1×10^{-3} M, this value lowered to 3.91 eV, while at 1×10^{-2} M it witnessed a reduction to 3.63 eV and at the final concentration of 1×10^{-1} M it was only about 3.21 eV.

At better band gap values at lower concentrations the films are amorphous & which is also authenticated through XDR results. Localized states and a broadening of the optical band gap are illustrated as sources of structural disorder in amorphous materials. With increasing precursor concentration, the films exhibit greater crystallinity, leading to improved structural ordering and electronic delocalization. As a result, structural disorder is significantly reduced, as well as grain growth which leads to the reduction of the band gap. The correlation between the used amount of precursor, the films crystallinity and energy band gap in made ZnS thin films in general are clearly shown by optical results.

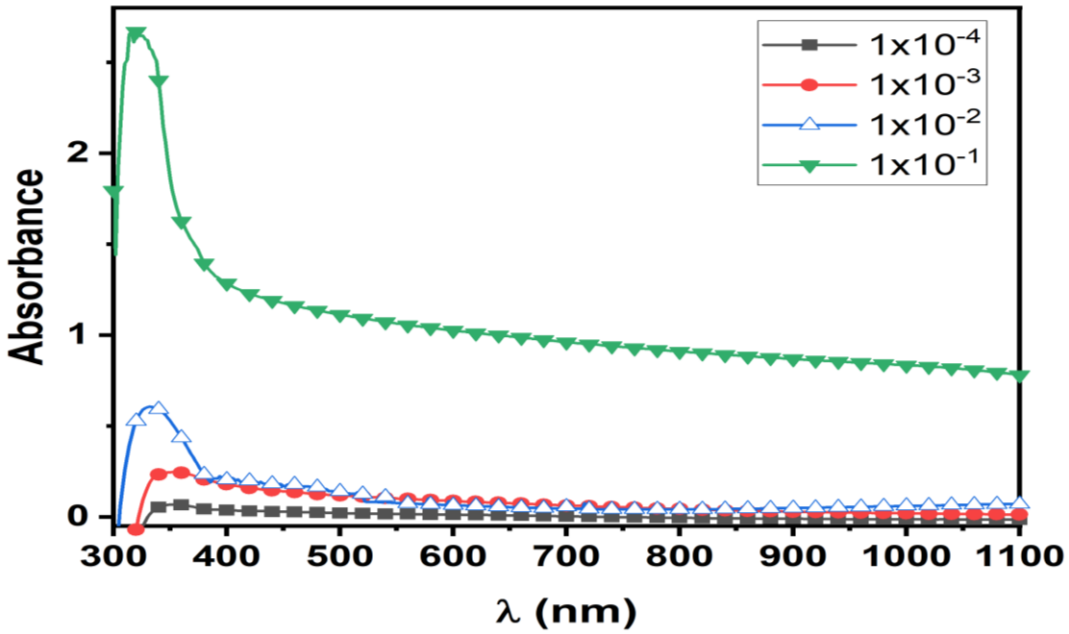

Figure 5: Absorbance spectra of ZnS thin films.

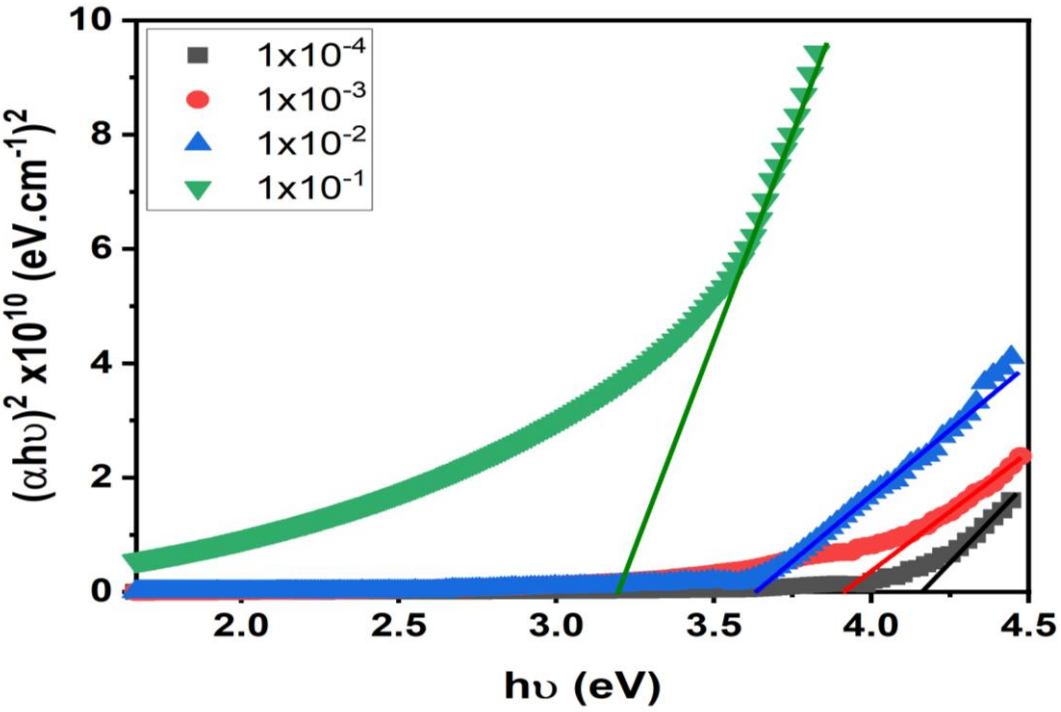

Figure 6: Band gap energy of ZnS thin films at different solution concentration.

Table 5: Band gap values of ZnS thin films

Sample	1×10^{-4}	1×10^{-3}	1×10^{-2}	1×10^{-1}
E_g (eV)	4.16	3.91	3.63	3.21

3.5. Fourier Transform Infrared Spectroscopy (FTIR)

Functional groups of deposited ZnS thin films were identified and chemical bonding was confirmed using Fourier transform infrared (FTIR) spectroscopy. Fig. 7 presents FTIR spectra of the samples. All samples showed a wide absorption band around 3441 cm^{-1} that is due to O–H stretching vibrations which might be related to absorbed humidity or OH groups on the film surface [29]. Specifically, the peaks appeared at 2914 cm^{-1} and 2847 cm^{-1} (especially clear for the 1×10^{-1} M sample) can be attributed to asymmetric and symmetric stretching modes of CH_2 groups [30], suggesting that residual organic species from precursor solution possibly exist in prepared materials. Both the absorption band located at 1601 cm^{-1} can be accounted for by C=O stretching vibrations and the peak detected in the region of 1456 cm^{-1} is due to asymmetric bending of CH_3 groups [31]. A band around 1431 cm^{-1} is connected to the symmetric stretching of zinc carboxylate (COO^-) groups [32], indicating decomposition products of zinc precursor. Furthermore, bands appearing around 714–719 cm^{-1} are designated as in plane rocking motions of (CH_2) groups. Notably, the characteristic Zn–S stretching vibrations were detected around 562 cm^{-1} and also in the range of 489–491 cm^{-1} [33], confirming that ZnS bonds indeed formed in these deposited films. As the precursor concentration increases further, improved ZnS formation and better consistency in chemical bonding leads to a more intense appearance of these Zn–S related peaks. Overall, the FTIR analysis not only affirms the successful growth of ZnS thin films but also suggests that even low amounts of residual organic groups can occur. The intensification of the Zn–S vibrational modes at higher concentrations is in accordance with the enhanced crystallinity found from XRD results

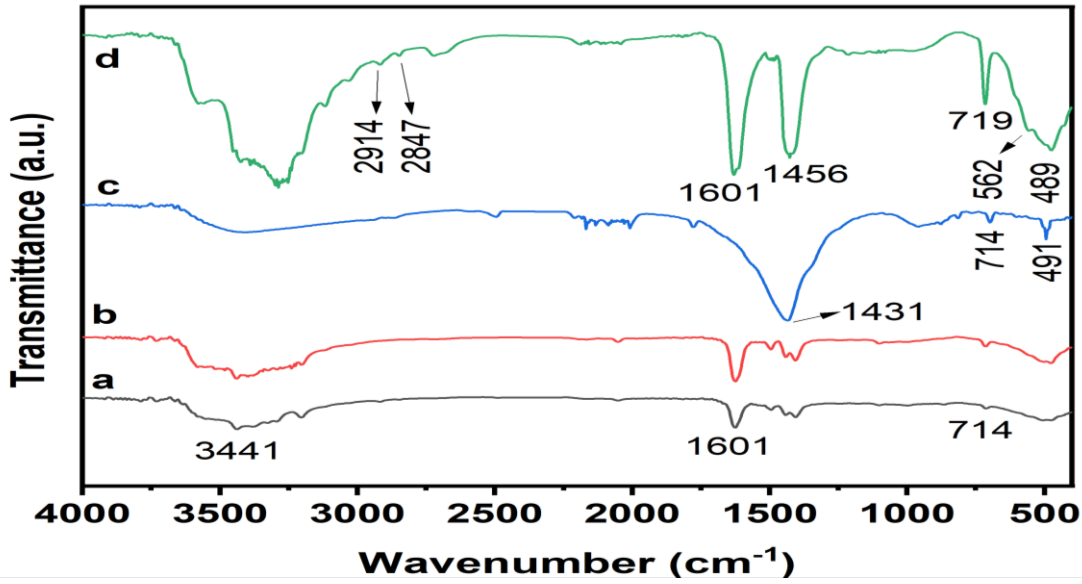

Figure 7: FTIR spectra of ZnS thin films at different precursors concentration: (a) 1×10^{-4}, (b) 1×10^{-3}, (c) 1×10^{-2} and (d) 1×10^{-1} mol of zinc chloride and thiourea.

4. Conclusions

ZnS thin films were deposited on glass substrates using the spray pyrolysis technique with different precursor concentrations. The findings indicate that precursor concentration is a parameter of choice that controls the structural, morphological, compositional and optical characteristics of the films. At lower concentrations, the non-crystalline structure observed by XRD became a distinct crystal shape as concentration increased. The increase in precursor, respectively, considerably increases the nucleation sites and allows the films to have smaller grains with smooth and homogeneous surface

of powders as confirmed by SEM and AFM observations. EDX analysis results indicated that increased precursor concentrations lead to lower oxygen incorporation, as well as higher formation of Zn–S bonds, thus improving the stoichiometry and film purity. Optical measurements revealed that using a higher concentration not only increased the amount of light that the films can absorb but also narrowed the band gap, which was consistent with better crystal quality in these films. In conclusion, the study indicates that varying precursor quantity is an effective way to enhance overall structural characteristics and optical properties of ZnS nanostructured thin films obtained via spray pyrolysis thus making this technique promising for optoelectronic applications.

Conflict of Interest

The authors declare no conflict of interest.

References

1. M. Alzaid, W.S.Mohamed, M. El-Hagary, E.R. Shaaban, N. M. Hadia, Optic. Mater., **118**, 111228 (2021). https://doi.org/10.1016/j.optmat.2021.111228.
2. T. Hurma, Materials Today: Proceedings, **18**, 1875 (2019). https://doi.org/10.1016/j.matpr.2019.06.676.
3. C. Wang, J. Li, W. Feng, Y. Ye, H. Guo, Optik, **242**, 167095 (2021). https://doi.org/10.1016/j.ijleo.2021.167095.
4. W.L.Liu, W.J.Chen, S.H.Hsieh, J.H.Yu, Procedia Engineering, **36**, 46 (2012). https://doi.org/10.1016/j.proeng.2012.03.009.
5. S.Wu, J.Zhao, Y.Zhao, K.Wang, W.Yang, H.Cheng, M. Li, Infrared Physics & Technology, **98**, 23 (2019). https://doi.org/10.1016/j.infrared.2018.12.009.
6. A.A.Adewale, A.Chik, T.Adam, T.M. Joshua, M.O.Durowoju, Materials Today Communications, **27**, 102077 (2021). https://doi.org/10.1016/j.mtcomm.2021.102077.
7. C. Sabitha, I.H.Joe, K.D.A.Kumar, S.Valanarasu, Optical and Quantum Electronics, **50**, 1(2018). https://doi.org/10.1016/j.ijleo.2017.10.034.
8. A.M.Al-Diabat, N.M.Ahmed, M.R.Hashim, M.A.Almessiere, Materials Today: Proceedings, **17**, 912(2019). https://doi.org/10.1016/j.matpr.2019.06.390.
9. A.Najim, B.Hartiti, H.Labrim, S.Fadili, P.Thevenin, M.Ertugrul, Materials Today: Proceedings, **66**, 249 (2022). https://doi.org/10.1016/j.matpr.2022.04.877.
10. A.Sundhar, Materials Today: Proceedings, **48**, 377(2022). https://doi.org/10.1016/j.matpr.2020.09.550.
11. H.Benamra, H.Saidi, A.Attaf, M.S.Aida, A.Derbali,N.Attaf, Surfaces and Interfaces, **21**, 100645(2020). https://doi.org/10.1016/j.surfin.2020.100645.
12. S.Palanichamy, J.R.Mohamed, P.S.Kumar, S.Pandiarajan, L.Amalraj, Optical and Quantum Electronics, **50**, 1(2018). https://doi.org/10.1007/s11082-018-1611-0.
13. K.D.A.Kumar, V.Ganesh, S.Valanarasu, M.Shkir, I.Kulandaisamy, A.Kathalingam, S.AlFaify, Materials Chemistry and Physics, **212**, 167 (2018). https://doi.org/10.1016/j.matchemphys.2018.03.035.
14. H.Pervaiz, Z.S.Khan, N.Shahzad, N.Ahmed, Q.Jamil, Materials Chemistry and Physics, **290**, 126602(2022). https://doi.org/10.1016/j.matchemphys.2018.03.035.
15. A.Kennedy, V.S.Kumar, K.P.Raj, Journal of Physics and Chemistry of Solids, **110**, 100 (2017). https://doi.org/10.1016/j.jpcs.2017.06.004.
16. A.Najim, B.Hartiti, H.Labrim, S.Fadili, P.Thevenin, M. Ertugrul, Materials Today: Proceedings, **66**, 249(2022). https://doi.org/10.1016/j.matpr.2022.04.877.
17. T.Amakali, L.Daniel, V.Uahengo, N.Y.Dzade, N.H.De Leeuw, Crystals, **10**, 132(2020). https://doi.org/10.3390/cryst10020132.
18. E.Veena, K.V.Bangera, G.K.Shivakumar, *In AIP Conference Proceedings* (*Vol. 1859, No. 1)*. AIP Publishing (2017). https://doi.org/10.1063/1.4990268
19. Z.K.Heiba, M.B.Mohamed, N.M.Farag, S.I.Ahmed, Crystal Research and Technology, **56**, 2000201 (2021). https://doi.org/10.1002/crat.202000201.
20. S.Munyai, S., N.C.Hintsho-Mbita, Current Research in Green and Sustainable Chemistry, **4**, 100163 (2021). https://doi.org/10.1016/j.crgsc.2021.100163.
21. A.T.Salih, A.A.Najim, M.A.Muhi, K.R.Gbashi, Optics Communications, **388**, 84 (2017). https://doi.org/10.1016/j.optcom.2016.12.035.

22. D.Mendil, F.Challali, T.Touam, A.Chelouche, A.H.Souici, S.Ouhenia, D.Djouadi, Journal of Luminescence, **215**, 116631(2019). https://doi.org/10.1016/j.jlumin.2019.116631.
23. H. Labiadh, K. Lahbib, S. Hidouri, S. Touil, and T. BEN Chaabane, Asian Pac J Trop Med, **9**, 757 (2016). https://doi.org/10.1016/j.apjtm.2016.06.008.
24. H. Qu, L. Cao, G. Su, W. Liu, R. Gao, C. Xia, J. Qin, Journal of Nanoparticle Research, **16**, 757 (2014). https://doi.org/10.1007/s11051-014-2762-y.
25. I. Daskalakis, I. Vamvasakis, I. T. Papadas, S. Tsatsos, S. A. Choulis, S. Kennou and G. S. Armatas, Inorg Chem Front, **7**, 4687 (2020). https://doi.org/10.1039/d0qi01013h.
26. H. K. Sharma, P. K. Shukla, and S. L. Agrawal, J Mater Sci: Mater Electron, **28**, 6226 (2017). https://doi.org/10.1007/s10854-016-6302-7.
27. K. A. Hubeatir, Eng. and Tech. J., **34**, 178 (2016). https://doi.org/10.30684/etj.34.1A.15.
28. I.A.Ezenwa and N.A.Okereke, Adv. Appl. Sci. Res., **3**, 2821(2012).
29. K. Bera, S. Saha, and P. C. Jana, Orient. J. Chem., **34**, 1665 (2018). https://doi.org/10.13005/ojc/340363.
30. R. Khan, N. S. Das, and K. K. Chattopadhyay, J Mater Sci: Mater Electron, **30**, 19189 (2019). https://doi.org/10.1007/s10854-019-02276-y.
31. L-N. Liu, J.-G. Dai, T.-J.Zhao, S-Y. Guo, D.-S.Hou, P.Zhang, J.Shang, S.Wang and S.Han, RSC Adv, **7**, 35075 (2017). https://doi.org/10.1039/c7ra04259k.
32. K. Nagamani, P. Prathap, Y. Lingappa, R. W. Miles, and K. T. R. Reddy, Phys Procedia, **25**, 137 (2012). https://doi.org/10.1016/j.phpro.2012.03.062.
33. M. K. Trivedi, R. M. Tallapragada, and A. Branton, J. Lasers Opt Photonics, **2**, 1000122 (2015), https://doi.org/10.4172/2469-410X.1000122.

تأثير التركيز على الخصائص التركيبية والضوئية لأغشية *ZnS* الرقيقة المرسبة بتقنية الانحلال الحراري بالرش

هبة كامل عبود[1] و نذيرة عباس علي[1]
[1]قسم الفيزياء، كلية العلوم، جامعة بغداد، بغداد، العراق

الخلاصة

تم ترسيب أغشية رقيقة من كبريتيد الزنك (ZnS) على ركائز زجاجية باستخدام تقنية التحلل الحراري بالرش (SPD) بتراكيز مختلفة من المادة الأولية (من 10^{-4} إلى 10^{-1} مولار). دُرست الخصائص البنيوية والمورفولوجية والتركيبية والبصرية باستخدام حيود الأشعة السينية (XRD) ومجهر القوة الذرية (AFM) ومجهر المسح الإلكتروني (SEM) ومطيافية تشتت طاقة الأشعة السينية (EDX) ومطيافية تحويل فورييه للأشعة تحت الحمراء (FTIR) ومطيافية الأشعة فوق البنفسجية والمرئية (UV-Vis). كشفت نتائج حيود الأشعة السينية عن تحول من بنية ZnS غير متبلورة إلى بنية مكعبة متبلورة مع زيادة تركيز المادة الأولية. أظهرت تحليلات FESEM وAFM أن التركيزات الأعلى تُنتج أسطحًا أكثر نعومة بأحجام جسيمات أصغر. أكدت مطيافية تشتت طاقة الأشعة السينية تحسنًا في التكافؤ الكيميائي عند التركيزات الأعلى. انخفضت فجوة النطاق البصري من 4.16 إلى 3.21 إلكترون فولت مع زيادة التركيز، مما يشير إلى تحسن التبلور. تُظهر النتائج أن تركيز المادة الأولية يؤثر بشكل كبير على الخصائص الهيكلية والبصرية للأغشية الرقيقة من كبريتيد الزنك.

الكلمات المفتاحية: غشاء ZnS الرقيق، تركيزات مختلفة، الانحلال الحراري بالرش، الخصائص التركيبية، الخصائص البصرية، فجوة النطاق.